CircCDR1 sponges miR-1290 to regulate cell proliferation, migration, invasion, and apoptosis in esophageal squamous cell cancer

Yong Fang, Jun Yin, Yaxing Shen, Hao Wang, Han Tang & Xiaosang Chen

View supplementary material

Published online: 15 Mar 2022.

Submit your article to this journal

Article views: 42

View related articles

View Crossmark data

Taylor & Francis
Taylor & Francis Group

RESEARCH PAPER

Check for updates

CircCDR1 sponges miR-1290 to regulate cell proliferation, migration, invasion, and apoptosis in esophageal squamous cell cancer

Yong Fang, Jun Yin, Yaxing Shen, Hao Wang, Han Tang, and Xiaosang Chen

Department of Thoracic Surgery, Zhongshan Hospital, Fudan University, Shanghai, China

ABSTRACT

Since circCDR1 was abnormally expressed in esophageal squamous cell cancer (ESCC), the current study explored whether circCDR1 affected ESCC. Detailedly, circCDR1 expression in ESCC and linear isoform and stability of circCDR1 were detected by RT-qPCR. The location of circCDR1 was detected by fluorescence *in situ* hybridization (FISH). After transfection, the cell biological functions were detected by wound-healing, CCK-8, colony formation, and flow cytometry assays. The target of circCDR1 was predicted by bioinformatics, FISH, RNA pull-down, and dual-luciferase reporter assays. The correlation between circCDR1 and miR-1290 was analyzed by Pearson's correlation analysis. A subcutaneous-xenotransplant tumor model in BALB/c nude mice was established and the levels of circCDR1, miR-1290, and apoptosis/metastasis/proliferation-related factors in the cancer cells and tissues were detected by immunohistochemical analysis, western blot, or RT-qPCR. As a result, circCDR1 was low-expressed in ESCC tissues and cells, while miR-1290 was high-expressed. CircCDR1 was regulated and was negatively correlated with miR-1290. CircCDR1, located in cytoplasm, inhibited the viability, proliferation, migration, and invasion of the cancer cells and the expressions of Bcl-2, N-cadherin, and Vimentin, but enhanced cell apoptosis and the expressions of C caspase-3, Bax, E-cadherin, IGFBP4, LHX6 and NFIX. *In vivo*, circCDR1 promoted xenotransplanted tumor weight and volume, and the expressions of C caspase-3 and Bax yet suppressed the levels of Bcl-2, miR-1290, and Ki-67 in tumor tissues. The effects of circCDR1 on both cancer cells and tissues were opposite to and reversed by miR-1290 mimic. Collectively, circCDR1 sponged miR-1290 to regulate the progression of ESCC both *in vitro* and *in vivo*.

Introduction

Esophageal cancer, principally comprising two pathological types (esophageal squamous cell cancer (ESCC) and esophageal adenocarcinoma), is a frequently diagnosed tumor in digestive system with approximate more than 456,000 new cases and over 400,000 deaths annually, making it a primary cause of cancer-related death all over the world [1,2] ESCC accounts for 90% of all cases of esophageal cancer globally [3], and is the dominant type of esophageal cancer in China [4]. Most patients with esophageal cancer have already developed into the advanced stage before diagnosis, as a result of unobvious symptoms of esophageal at early stage of the disease [2]. Despite the innovative development of esophageal cancer treatment, five-year survival of esophageal cancer patients is still as low as 21%

[2,5]. The development of esophageal cancer is associated with the abnormally regulated multiple genes including oncogenes, and tumor suppressor [6,7]. Hence, to identify genes involved in the prevention and diagnosis of ESCC is of great value.

Circular RNAs (circRNAs) are highly tissue-specific and stable [8,9]. More than 10% of the expressed mRNAs produce circRNAs whose expressions are 10 times their respective host gene expressions [10]. Scientists have reported that circRNAs are involved in a wide range of physiological or pathological processes in different kinds of diseases [10–12]. In addition, increasing evidence has indicated that circRNAs could regulate the proliferation, apoptosis, and metastasis of cancer cells and angiogenesis, suggesting that circRNAs may become novel biomarkers for the

---

prevention and treatment of many cancers [10,13,14]. For instance, circPDSS1 promotes the progression of bladder cancer [15]; circUCK2 inhibits the proliferation and invasion of prostate cancer cells [16]; circ-100,395 also could inhibit ovarian cancer cells to proliferate and metastasize [17]; and aberrantly expressed circCDR1 in many cancers has regulatory effects on the biological functions of cancer cells, including lung cancer cells and glioblastoma cells [18,19]. Recently, circCDR1 has been found to be low-expressed in esophageal cancer [9]. However, to the best of our knowledge, no research has been conducted on the impact of circCDR1 on ESCC.

The purpose of this study was to investigate the influence of circCDR1 in ESCC and to further clarify the potential mechanism.

Methods

Tissue samples and ethics statement

ESCC tissues and adjacent normal tissues (ANT) were collected from 60 patients with ESCC during surgical resection performed at Zhongshan Hospital, Fudan University between December 2018 and March 2019. The major clinicopathological features of patients, including gender, age, tumor size, differentiation, lymph node metastasis and Tumor-Node-Metastasis (TNM) stage, were obtained from the Zhongshan Hospital, Fudan University. The study and animal experiments were ratified by the Ethics Committee (Z20181211S) and Committee of Experimental Animals (Z20190721S) of Zhongshan Hospital, Fudan University. All patients have signed the written informed consent. All the experiments in the current study were performed at Zhongshan Hospital, Fudan University.

Cell culture

Human esophageal epithelial cell line Het-1A (BFN60806666) was obtained from Blue F Bio (http://www.bluefcell.com/productinfo/116090.html). Human ESCC cell lines EC9706 (Jennio, Guangzhou, China, http://www.jennio-bio.com/), KYSE-220 (CSC-C6799J, Creative Bioarray, NY, USA, https://www.creative-bioarray.com/), TE-9

(BNCC351845, BNBIO, Beijing, China, http://www.bnbio.com/Product/BNCCSearch?key=%20TE-9), as well as KYSE-150 and KYSE-30 (CL-0638; CL-0577, Procell, Wuhan, China, https://www.procell.com.cn/Index/search.html?keyword=CL-0638) were acquired. All cells were grown in RPMI 1640 medium (C11875500BT, Gibco, MA, USA) containing 10% Fetal Bovine Serum (FBS, 16,140,071, Gibco) and incubated at 37°C in a humid environment with 5% CO_2.

RNA extraction

MiRNAs were isolated from clinical tissues, mice tumor tissues and esophageal cancer cells using EasyPure miRNA Kit (ER601-01, TransGen Biotech, Beijing, China). The tissue samples were ground into pieces by a grinding rod and lysed by lysis buffer. The cells were directly lysed by a lysis buffer. Then, 200 μl chloroform (YZ-1601383, Solarbio, Beijing, China) was mixed with the lysates of tissues and cells, followed by being centrifuged (13,000 × g) for 30 min to collect the miRNAs and washed with 75% ethanol (E111991, Aladdin, Shanghai, China) once. After the removal of the ethanol by another 15-min centrifugation (13,000 × g), the miRNAs were diluted by RNase-free H_2O (RF001, Real-Times, Beijing, China).

Cytoplasm and nuclear RNAs were extracted from the esophageal cancer cells using Cytoplasmic & Nuclear RNA Purification Kit (37,400, AmyJet Scientific Incorporation, Wuhan, China) (http://www.amyjet.com/products/NGB-37400.shtml). In brief, 3×10^6 cells were incubated with Lysis Buffer J in a 1.5 ml centrifugal tube and centrifuged (14,000 × g) for 10 min. Then the supernatant was collected for extracting cytoplasm RNAs, and the sediments were harvested for isolating cytoplasm RNAs extraction. The supernatant and sediments were separately mixed with Buffer SK (200 μl for supernatant and 400 μl for sediment) for 10 s, and then added with 200 μl 100% ethanol. Next, the mixture was transferred into a rotating column that had already been assembled with a collecting tube, and centrifuged for 1 min (3500 × g). The rotating column was further assembled with new elution tube. Finally, 50 μl Elution Buffer E was added into the rotating column, and the cytoplasm and nuclear RNAs

were collected by centrifuging (14,000 × *g*) for 1 min.

Total RNAs were separated from the tumor tissues and cells. The tissues and cells were incubated with TRIzol (15,596, Invitrogen, MA, USA) and chloroform, then centrifuged (14,000 × *g*) for 20 min, and further cultured with isopropanol (H822173, Macklin, Shanghai, China). Finally, the RNAs were washed with 75% ethanol and diluted by RNase-free H_2O.

Reverse transcription quantitative polymerase chain reaction (RT-qPCR)

The RNAs were reverse-transcribed into cDNAs by EasyScript First-Strand cDNA Synthesis SuperMix (AE301-02, TransGen Biotech) following the instructions. PerfectStart Green qPCR SuperMix (AQ601-01, TransGen Biotech) was mixed with the cDNAs and the gene primers to amplify the cDNAs in QuantStudio6 system (Applied Biosystems, CA, USA). Finally, the RNA expression level was quantified using the $2^{-\Delta\Delta CT}$ method. The primer sequences were listed in Table 1.

RNase R and actinomycin D treatments

For RNase R treatment, RNAs were extracted and collected from KYSE-30 and TE-9 cells, and then 2.5 μg RNAs were incubated with 40 U RNase R reagent (M1228, BioVision Incorporated, CA, USA) at 37°C for 30 min. The treated RNAs were prepared for RT-qPCR to examine the linear isoform of circCDR1.

For actinomycin D treatment, the KYSE-30 and TE-9 cells were first cultured in the complete medium with 2 mg/ml actinomycin D (A9415, Sigma, Beijing, China) for 24 h. Then the cells were collected for extracting RNAs, which were used in RT-qPCR for detecting the stability of circCDR1.

Cell transfection

Small interfering RNA for circCDR1 (si-circCDR1; 5'-ACGUUAUAGGUCCCAAAGGC-3'), and circCDR1 overexpression plasmids ligated into pLVX-cir vector were synthesized from GenePharma (Shanghai, China). Plasmids without any target sequence served as negative controls (NC). MiR-1290 mimic (miR10005880-1-5; 5'-UGGAUUUUUGGAUCAGGGA-3') and the mimic control (MC; miR1N0000002-1-5; 5'-UUCUCCGAACGUGUCACGUUU-3') were synthesized by RIBOBIO (Guangzhou, China).

Prior to transfection, KYSE-30 (2.5×10^6) and TE-9 (2.5×10^6) cells in the 2 ml complete medium were plated into 6-well plates and cultured to approximately 70% confluence. Two micrograms of plasmids, siRNA, or mimic and 3 μl Lipo2000 (P-lipo, Promoter, Wuhan, China) were diluted by

Table 1. RT-qPCR primers.

Target gene	Forward primers, 5'-3'	Reverse primers, 5'-3'
CircCDR1	TCCAGTGTGCTGATCTTCTGAC	GGTCTATTAGGACTCGAAGGT
miR-1290	CGGGACATAGTCAGCAGTG	GCTGGGCACAGATGATTTTG
CDR1	ACGTCTCCAGTGTGCTGA	CTTGACACAGGTGCCATC
miR-490-5p	GTCTACAAGGGCATCTGGAT	GTGGATGTCAGGCAGATGC
miR-1246	ATCCTACCAGACCCTTCAGTG	GCCAGACGAGACCAATCATC
miR-671-5p	CCGCCGCACTGACAGTATGC	AGGGTCCCCAAGAGGAGAAG
miR-7	CATGTCTGGTAACGGCAATG	GTACGAGGCTTTCAATGTTG
Bcl-2	GGTGGGGTCATGTGTGTGG	CGGTTCAGGTACTCAGTCATCC
Bax	CCCGAGAGGTCTTTTTCCGA	CCAGCCCATGATGGTTCTGAT
E-Cadherin	CGAGAGCTACACGTTCACGG	GGGTGTCGAGGGGAAAAATAGG
N-Cadherin	TCAGGCGTCTGTAGAGGCTT	ATGCACATCCTTCGATAAGACTG
Vimentin	GACGCCATCAACACCGAGTT	CTTTGTCGTTGGTTAGCTGGT
SCAI	AAGCAGTGGCAGTCCTATTTTG	GCTTCAAGCCATACCGATTATCC
IGFBP3	AGAGCACAGATACCCAGAACT	GGTGATTCAGTGTGTCTTCCATT
INPP4B	CCAGAAGACTCCAAATGAACCG	ACGGGGTGGATTACGGAGA
LHX6	GGGCGCGTCATAAAAAGCAC	TGAACGGGGTGTAGTGGATGT
IRF2	CATGCGGCTAGACATGGGTG	GCTTTCCTGTATGGATTGCCC
NFIX	CGGCTCTACAAGTCGCCTC	GCAGTGGTTTGATGTCCGC
U6	CTCGCTTCGGCAGCACA	AACGCTTCACGAATTTGCGT
GAPDH	AGGTCGGTGTGAACGGATTTG	GGGGTCGTTGATGGCAACA

100 μl medium without FBS. The diluted plasmids, siRNA or mimic was incubated with the diluted Lipo2000 for 15 min at room temperature, and then further added into 6-well plates, with each well containing 1.8 ml fresh medium. Another 48-h culture later, the cells were harvested for later use.

Cell counting kit-8 (CCK-8) assay

CCK-8 (APExBIO, Houston, USA) was used to detect cell viability. After the transfection of KYSE-30 and TE-9 cells, the cells (1.0×10^4) in 100 μl complete medium were seeded into each well of a 96-well plate to culture for 24 h or 48 h, followed by the addition of 5 mg/ml 10 μl CCK-8 solution into each well and 4-h incubation. Finally, a microplate reader (Imark, Bio-Rad, CA, USA) was used to read the absorbance at 540 nm.

Biotinylated RNA pull-down assay

To pull down circCDR1 in miRNAs, the C-1 magnetic beads (C37488, Life Technologies, CA, USA) were incubated with biotinylated-circCDR1 probe (61,002, Life Technologies), and then the probe-coated beads were further cultivated with sonicated KYSE-30 and TE-9 cells at 4°C overnight. The next day, after eluting the probe-coated beads, the rest samples were subjected to RT-qPCR to detect the expressions of miRNAs with circCDR1 pull-down.

For miR-1290 pulled down by circCDR1, circCDR1 was overexpressed in KYSE-30 and TE-9 cells, which were then transfected with biotinylated miR-1290-WT or miR-1290-MUT using Lipo2000. Next, the cells were collected, lysed, sonicated, and further incubated with C-1 magnetic beads at 4°C overnight. The next day, after the probe-coated beads were eluted, the rest samples were subjected to RT-qPCR for detecting the expression of miR-1290 with circCDR1 pull-down.

Dual-luciferase reporter assay

CircCDR1 sequences with wide-type (CircCDR1-WT) (5'-ATCCTGACTTCCAGAAAATCCA-3') or mutant (CircCDR1-MUT) (5'-ATCCTGACTTCCAGTGCTAATC-3') containing

miR-1290 binding sites were inserted into pmirGLO luciferase Vectors (E1330, Promega, CA, USA). KYSE-30 (3.0×10^4) and TE-9 (3.0×10^4) cells were seeded in 48-well plates, which were supplemented with 300 μl complete medium overnight, subsequent to which the KYSE-30 and TE-9 cells were transfected with the vectors and miR-1290 mimic together. After the transfection, the cells were subjected to dual-luciferase reporter assay kit (ab228530, Abcam, CA, USA). Ultimately, the luciferase activity of cells was examined under GloMax fluorescence reader (Promega).

Fluorescence in situ hybridization (FISH)

The RNA FISH assay was conducted using Fluorescent In Situ Hybridization Kit (C10910, RIBOBIO) to determine the expression location of circCDR1 (detected in KYSE-30 cells) and the co-location of circCDR1 and miR-1290 (detected in TE-9 cells) as per the manufacturer's protocol. The sequence of circCDR1 was 5'-CCATCGGAAACCCTGGATATTGCA-3'. The KYSE-30 (2.0×10^5) and TE-9 (2.0×10^5) cells were seeded into 6-well plates. After the cells adhered to the bottom of each well, Cy3-labeled circCDR1 probes or Dig-labeled locked nucleic acid miR-1290 probes (miRB0005880-2-1, RIBOBIO) were used to label the cell nuclei using the Fluorescent In Situ Hybridization Kit. Finally, the cells were observed and recorded with a confocal fluorescence microscope (FV3000, OLYMPUS, Japan)

Colony formation assay

Post the transfection, KYSE-30 (2×10^2) and TE-9 (2×10^2) cells were inoculated into 6-well plates with 2 ml complete medium and cultured for 14 days. After the removal of the medium, 4% formaldehyde (P804536, Macklin) was added into each well to incubate the cell colonies for 10 min. Then, the formaldehyde was removed, and the cell colonies were stained by 0.3% crystal violet for 15 min, followed by removing crystal violet and washing three times with phosphate buffered saline (PBS). The number of colonies in each well was analyzed by Image J 1.8.0 software.

Wound healing assay

3.0×10^5 transfected KYSE-30 and TE-9 cells were added into each well of 6-well plates supplemented with a 2 ml complete medium. When the confluence reached about 95%, a wound with the same width was created by scratching in the surface of cells of each well, and the medium was then replaced by a medium without FBS. The wound in the cells of each well was photographed at 0 and 48 h using an optical microscope (DM4M, Leica, Solms, Germany). The data were analyzed using the Image J 1.8.0 software.

Transwell assay

The 24-well Transwell chamber (pore size 8 μm) for invasion detection was purchased from Corning Life Sciences (NY, USA). In a nutshell, a 0.2 ml non-FBS medium containing transfected KYSE-30 (2.0×10^4) or TE-9 cells (1.5×10^4) was added into the upper Transwell chamber pre-coated with Matrigel, and 0.7 ml complete medium was added into lower chamber as a chemoattractant for 48-h incubation. Next, the cells remaining on the inner layer of the upper chambers were removed, while the cells that invaded to the lower chamber surface were fixed with 4% paraformaldehyde for 30 minutes (min) and stained with 1% crystal violet (C110704, Aladdin) at room temperature for 15 min. The invaded cells were observed under an optical microscope. Image J 1.8.0 software was used to count the cell numbers invaded into the lower chamber.

Flow cytometry

Flow cytometry was implemented to test the apoptosis of KYSE-30 and TE-9 cells by an Annexin V/PI kit (E606336, Sangon Biotech, Shanghai, China). Briefly, the transfected cells (2.0×10^5) in 2 ml of complete medium were added into a 6-well plate and cultured for 24 h. Then Annexin V and Propidium Iodide (PI) were applied to incubate the cells for 20 min in the dark. The cell fluorescence was evaluated by fluorescence-activated cell sorting caliber (FACSCaliburTM, BD Biosciences, San Jose, CA, USA).

Animals and subcutaneous xenograft

Sixty-four male BALB/c nude mice (age: 6 weeks old, weighting 20–22 g) were acquired from SLAC Laboratory Animal Technology (Shanghai, China). Mice were group-housed (2–5 per cage) and maintained group-housed on a 12 h/12 h light dark cycle at 25°C under specific pathogen-free (SPF) conditions. Care was taken to minimize pain and discomfort for the animals. KYSE-30 cells (2×10^6) or TE-9 cells (2×10^6) mixed with PBS and Matrigel (354,248, Corning Life Sciences) were subcutaneously injected into 32 mice via the right flank area. The body weight and tumor size were measured every day, and tumor volume was calculated according to the following formula: Tumor volume = major diameter (L) × (minor diameter)^2 (W^2) × π/6. After the volume of tumor in each mouse reached 100 mm^3, the mice were randomly divided into four groups: NC+MC (n = 16), circCDR1+ MC (n = 16), NC+M (n = 16), and circCDR1 + M groups (n = 16). Eight mice in each group were injected with KYSE-30 cells, while another eight mice were injected with TE-9 cells.

For NC+MC group, the tumors of the mice were injected with negative control plasmids and mimic control every 2 days. For circCDR1+ MC group, the tumors of the mice were injected with circCDR1 plasmids and mimic control every 2 days. For NC+M group, the tumors of the mice were injected with negative control plasmids and miR-1290 agomir (miR40005880-4-5, RIBOBIO) every 2 days. For circCDR1 + M group, the tumors of the mice were injected with circCDR1 plasmids and miR-1290 agomir every 2 days. Four weeks later, the mice were anesthetized by 2% sodium pentobarbital (B005, Jiancheng, Nanjing) at 50 mg/kg and sacrificed by cervical dislocation, subsequent to which the tumor tissues of all mice were harvested and weighed. In order to minimize the subjective bias, we will ensure that evaluation and statistical analysis are performed by the researchers who were unaware of the grouping.

Immunohistochemical assay

The tumor tissues were embedded in paraffin (S25190, Yuanye, Shanghai, China) and cut into

4-μm-thick slices with microtome (RM2235, Leica, Solms, Germany). The slices were fixed on a glass slide, deparaffinized, and incubated with an antigen repair solution (p0081, Beyotime) and endogenous peroxidase blocker (BF06060, Biodragon, Beijing, China) at room temperature for 10 min. After being blocked with 5% FBS, the tissues were incubated with Ki-67 antibody (1:500, ab15580, Abcam) at 4°C overnight. Then, the tissue slides were incubated with secondary antibody (G-21234, 1:500, Thermo Scientific) and Diaminobenzidine (DAB) reagent (SFQ004, 4A Biotech, Beijing, China) for 30 min. After the sections were stained by hematoxylin (B25380, Yuanye) for 10 min, the indexes were detected under an optical microscope (DM4M, Leica, Solms, Germany).

Western blot assay

NP-40 (P0013F, Beyotime) was used to lyse the cells and tumor tissues to acquire total proteins. After the protein concentration was determined by a bicinchoninic acid (BCA) kit (P0009, Beyotime), 25 μg total proteins were separated by SDS-PAGE gels (P0052A, Beyotime) and then transferred to nitrocellulose filter membranes (HTS112M, Millipore, MA, USA). A 2 μl marker (PR1910, Solarbio, Beijing, China) was also added into one lane on the SDS-PAGE gels and then transferred to nitrocellulose filter membranes in parallel. All membranes were blocked with 5% no-fat milk for 1.5 h and further incubated with the primary antibodies against C caspase-3 (1:2500, 17 kDa, ab2302, Abcam), Bcl-2 (1:2000, 26 kDa, ab59348, Abcam), Bax (1:3000, 33 kDa, ab32503, Abcam), E-Cad (1:2000, 97 kDa, ab40772, Abcam), N-Cad (1:1000, 130 kDa, ab18203, Abcam), Vimentin (1:2000, 54 kDa, ab92547, Abcam), IGFBP3 (1:4000, 32 kDa, ab77635, Abcam), LHX6 (1:1000, 50 kDa, ab22885, Abcam), NFIX (1:1000, 55kD, ab101341, Abcam) and GAPDH (1:5000, 36 kDa, ab8245, Abcam) overnight, followed by the cultivation with the secondary antibody Goat Anti-Rabbit IgG H&L (1:5000, ab205718, Abcam) for 1.5 h at room temperature the next day. Finally, after the surfaces of each membrane was covered by developer solution (P0019, Beyotime), the signal of membranes and the densitometric analysis of proteins were analyzed by Image Lab 3.0 Software (Bio-Ras, CA, USA).

Statistical analysis

Student's t-test and one-way analysis of variance (ANOVA) were used to analyze the data under SPSS 20.0 software. Kolmogorov–Smirnov test was used to verify normality. The least significant difference (LSD) and Dunnet's tests were used as post-hoc tests and the correlation of miR-1290 with circCDR1 expression was examined by Pearson's correlation analysis. Overall survival (OS) and disease-free survival (DFS) were calculated using Kaplan–Meier survival analysis. Survival data were estimated using the univariate and multivariate Cox proportional hazards model. Mean ± standard deviation (SD, n = 3) represented the final statistical data. A significant result was defined by $P < 0.05$.

Results

CircCDR1 was low-expressed in ESCC tissues and cells, as a prognostic biomarker

The clinical tissues were collected to examine the relationship between the expression of circCDR1 and clinicopathological features of tissues. The data revealed that the tumor differentiation of patients with negative circCDR1 expression (the negative or positive expression of circCDR1 in cancer tissues was defined by median) was poorer than that with positive circCDR1 expression, but the comparative results were opposite when it came to tumor invasion (Table 2). Then, we detected the expression of circCDR1 in esophageal cancer, as shown in Figure 1(a) that circCDR1 expression was down-regulated in Cancer group compared with that in ANT group. As for overall survival (OS) and disease-free survival (DFS) predictions, the two indexes were much lower in patients of Low circCDR1 group (according to the median level) than those of High circCDR1 group (Supplementary

Table 2. Relationship between circCDR1 expression and clinico-pathological features of ESCC.

Characteristics		n	circCDR1 expression		P value
			Negative	Positive	
Gender	Male	34	18	16	0.602
	Female	26	12	14	
Age	<60	32	18	14	0.301
	≥60	28	12	16	
Tumor size (cm)	<4	33	20	13	0.069
	≥4	27	10	17	
Differentiation	Well	22	4	18	<0.001
	Moderate	25	13	12	
	Poor	13	13	0	
Tumor invasion (T)	T1-T2	22	5	17	0.001
	T3-T4	38	25	13	
Lymph node metastasis	Absent	18	6	12	0.091
	Present	42	24	18	
TNM stage	I+ II	22	8	14	0.108
	III+IV	38	22	16	

Figure 1AB). Moreover, Table 3 displayed the associations of OS and DFS with age, tumor size, poor histological differentiation, tumor invasion, lymph node metastasis, advanced TNM stage and circCDR1 expression in patients with ESCC. Cox regression analysis confirmed the independent prognostic value of circCDR1 in BC patients (Table 3).

In addition, circCDR1 expression in ESCC cell lines was also evidently reduced as compared with that in normal cells (Figure 1(b)). As the

circCDR1 expression in KYSE-30 and TE-9 was the lowest, the two cell lines were singled out for later studies. We also found that in KYSE-30 and TE-9 cells, circCDR1 expression did not change under the incubation with RNase R or not, while CDR1 mRNA expression was markedly decreased under the incubation with RNase R than without RNase R (Figure 1(c)), which confirmed that circCDR1 harbored a loop structure. The stability of circCDR1 (Figure 1(d)) was also examined. After the actinomycin D (transcription inhibitor) treatment, the half-life of circCDR1 exceeded 24 h, while that of linear CDR1 was only about 4 h, indicating that circCDR1 was highly stable. Furthermore, regarding the location of circCDR1 in KYSE-30 cells (Figure 1(e)), the results of FISH demonstrated that the circCDR1 was mainly located in the cytoplasm.

CircCDR1 inhibited the viability, proliferation, migration, invasion and induced the apoptosis of KYSE-30 and TE-9 cells

CircCDR1 overexpression plasmids were transfected into KYSE-30 and TE-9 cells (Figure 2(a)), and the results revealed that the expression of circCDR1 was prominently enhanced but that of CDR1 did not change. Then we further detected

Table 3. Univariate and multivariate analysis of prognostic factors for DFS and OS in patients with esophageal squamous cell cancer.

Univariate and multivariate analysis of factors for OS and DFS in patients

Characteristics	Univariate analysis (DFS)		Multivariate analysis (DFS)		Univariate analysis (OS)		Multivariate analysis (OS)	
	HR (95% CI)	p value	HR (95% CI)	p value	HR (95% CI)	p value	HR (95% CI)	p value
Gender (Male/Female)	0.847 (0.454–1.582)	0.603	-	-	0.862 (0.430–1.729)	0.676	-	-
Age (<60/≥60)	1.034 (0.554–1.929)	0.917	-	-	0.959 (0.478–1.923)	0.905	-	-
Tumor size (<4 cm /≥4 cm)	0.768 (0.412–1.432)	0.406	-	-	0.512 (0.254–1.032)	0.061	-	-
Differentiation (Well/Moderate/Poor)	6.235 (2.516–15.476)	<0.001	2.443 (0.665–8.976)	0.18	3.383 (2.015–5.68)	<0.001	1.552 (0.772–3.117)	0.217
Tumor invasion (T1-T2/T3-T4)	4.499 (2.095–9.661)	<0.001	2.499 (0.792–7.884)	0.118	5.352 (2.161–13.256)	<0.001	4.567 (1.403–14.87)	0.012
Lymph node metastasis (Absent/Present)	1.592 (0.777–3.259)	0.204	-	-	1.415 (0.652–3.073)	0.38	-	-
TNM stage (I+ II/III+IV)	1.723 (0.858–3.460)	0.126	-	-	2.198 (0.982–4.918)	0.055	-	-
circCDR1 (Low/High)	0.334 (0.169–0.661)	0.002	0.39 (0.175–0.868)	0.021	0.237 (0.108–0.522)	<0.001	0.222 (0.081–0.607)	0.003

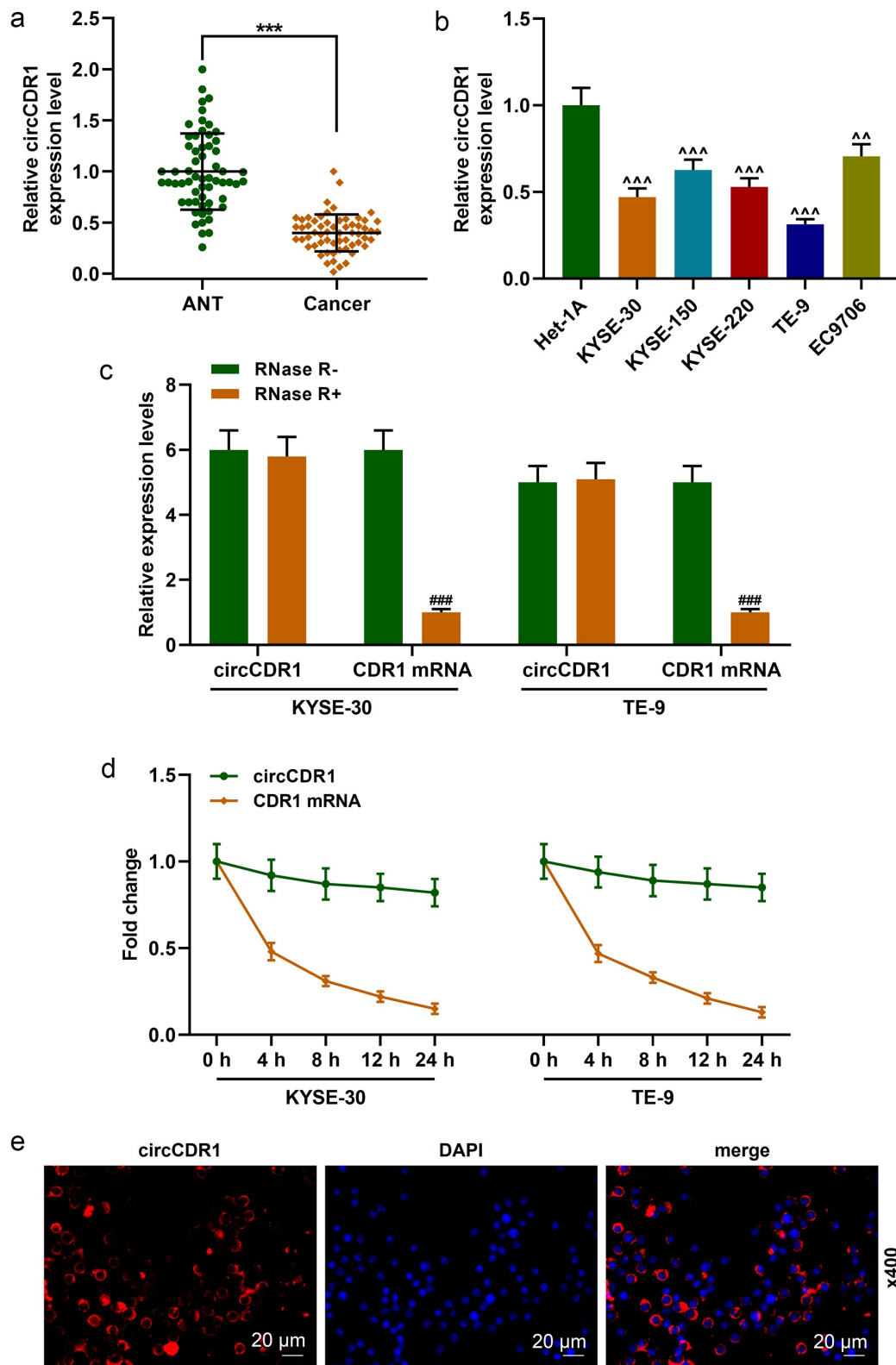OS, overall survival; DFS, disease-free survival.

Figure 1. CircCDR1 was low-expressed in ESCC tissues and cells. (a) The expression level of circCDR1 in ANT and ESCC tissues was analyzed by RT-qPCR. GAPDH was used as an internal control. (b) The expression level of circCDR1 in ESCC cell lines (KYSE-30, KYSE-150, KYSE-220, TE-9, and EC9706) and human normal esophageal epithelial cell line (Het-1A) was analyzed by RT-qPCR. GAPDH was used as an internal control. (c) CircCDR1 harboring a loop structure of in KYSE-30 and TE-9 cells treated with or without RNase R was detected by RT-qPCR. GAPDH was used as an internal control. (d) The stability of circCDR1 in KYSE-30 and TE-9 cells treated with actinomycin D was detected by RT-qPCR. GAPDH was used as an internal control. (e) The location of circCDR1 was detected by FISH in KYSE-30 cells. All experiments were conducted three times. (***$P < 0.001$, vs. ANT; ^^^$P < 0.001$, ^^$P < 0.01$, vs. Het-1A; ###$P < 0.001$, vs. RNase R–). (ESCC: squamous cell cancer, ANT: adjacent normal tissues, FISH: fluorescence in situ hybridization).
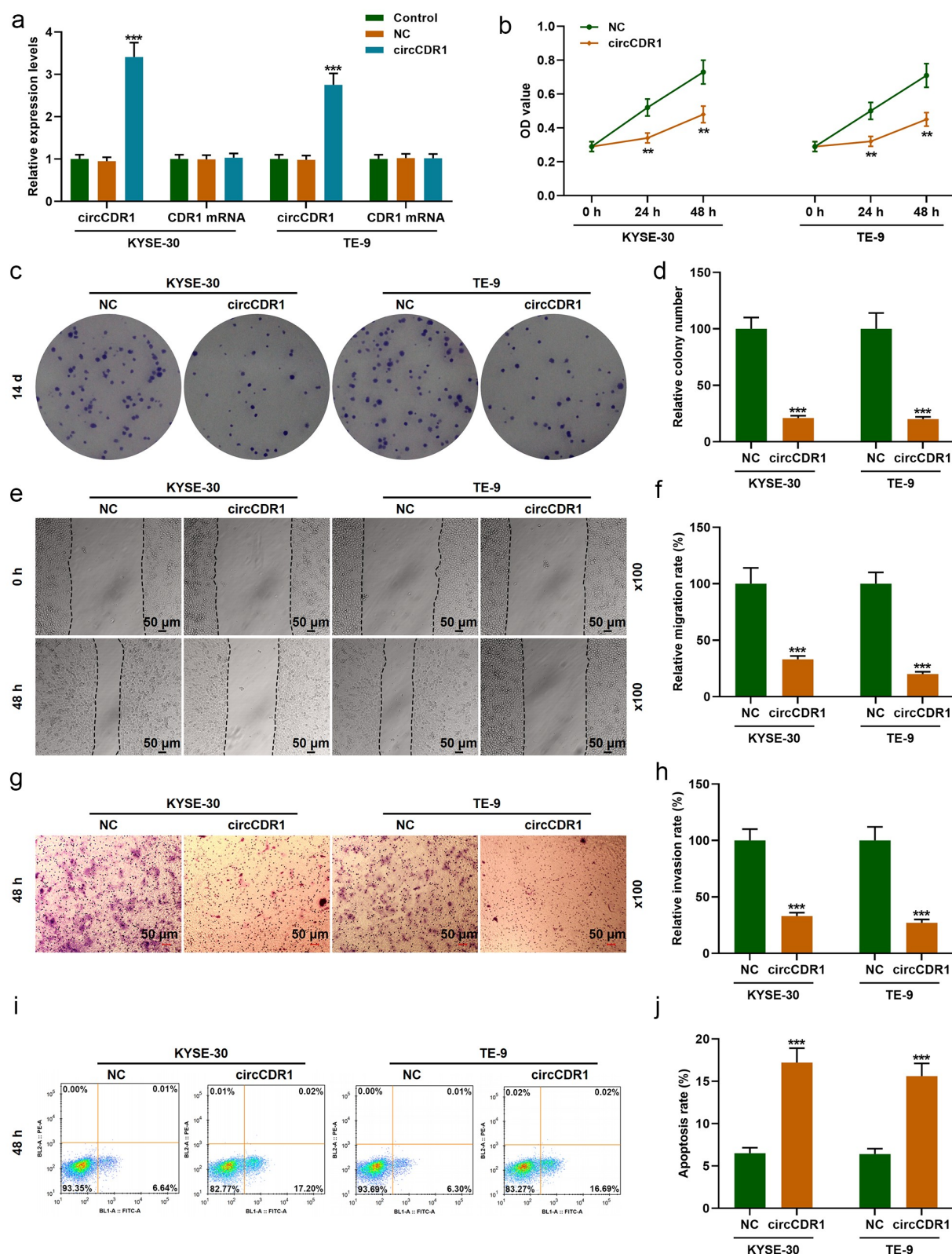
Figure 2. CircCDR1 inhibited the viability, proliferation, migration and invasion and induced the apoptosis of KYSE-30 and TE-9 cells. (a) The expressions of circCDR1 and CDR1 in KYSE-30 and TE-9 cells transfected with circCDR1 overexpression plasmids were detected by RT-qPCR. GAPDH was used as an internal control. (b) The cell viabilities of KYSE-30 and TE-9 cells after transfection were detected by CCK-8 assay. (c–d) The proliferation of KYSE-30 and TE-9 cells after transfection was detected by colony formation assay. (e–f) The migration of KYSE-30 and TE-9 cells after transfection was detected by wound-healing assay. (g–h) The invasion of KYSE-30 and TE-9 cells after transfection was detected by transwell assay. (i-j) The apoptosis of KYSE-30 and TE-9 cells after transfection was detected by flow cytometry. All experiments were conducted three times ($**P < 0.01$, $***P < 0.001$, vs. NC). (NC: Negative control).

the regulatory effects of circCDR1 on the biological functions of the two cells. CircCDR1 inhibited the viabilities after culture for 24 h and 48 h (Figure 2(b)), the numbers of colonies (Figure 2(c–d)), and the relative migration and invasion rates (Figure 2(e–h)), but promoted the relative apoptosis rate in the two cells (Figure 2(i–j)).

CircCDR1 was mainly located in cytoplasm and could capture miR-1290 in KYSE-30 and TE-9 cells

In order to further confirm the location of circCDR1, the nuclear and cytoplasm RNAs of the two cells were extracted and RT-qPCR was conducted, the findings of which indicated that circCDR1 was mainly expressed in cytoplasm both of KYSE-30 and TE-9 cells (Figure 3(a)). To further investigate whether the function of circCDR1 was correlated to miRNAs, a 3′ terminal-biotinylated-circCDR1 probe was synthesized (Figure 3(b)), and RNA pull-down assay was performed to determine the miRNAs potentially interacted with circCDR1. As depicted in Figure 3(c), only miR-1290 expression in both cells was greatly up-regulated among the 5 miRNAs. The result was further verified in Figure 3(d), in which miR-1290 was observably pulled down in KYSE-30 and TE-9 cells by a circCDR1 probe. The above data manifested that circCDR1 could capture miR-1290 in KYSE-30 and TE-9 cells.

CircCDR1 sponged high-expressed miR-1290 in ESCC tissues

MiR-1290 was predicted to be able to bind with circCDR1 (Figure 4(a)). To further confirm that circCDR1 could act as a sponge of miR-1290, the dual-luciferase reporter assay was carried out (Figure 4(b)). The co-transfection with miR-1290 mimic and circCDR1-WT caused diminished luciferase activities of the two cells, while the transfection of miR-1290 mimic and circCDR1-MUT did not result in difference, verifying that cirCDR1 could bind with miR-1290. Furthermore, the results of FISH expounded that circCDR1 did bind with miR-1290 in the cytoplasm of TE-9 cells (Figure 4(c)). The expression of miR-1290 in the two cells after overexpression or knockdown of circCDR1 (Figure 4(d–e)) was determined, which demonstrated that miR-1290 expression was obviously up-regulated by si-circCDR1 but down-regulated by circCDR1. The expression of miR-1290 was also enhanced in ESCC tissues (Figure 4(f)) and was negatively correlated with circCDR1 expression both in ANT and cancer tissues (Figure 4(g–h)).

MiR-1290 reversed the effects of circCDR1 on the proliferation, migration, invasion, apoptosis, and miR-1290 expression in KYSE-30 and TE-9 cells

The proliferation of the two cells was hindered by circCDR1 overexpression and boosted by miR-1290 mimic, while after the co-transfection of circCDR1 overexpression plasmids and miR-1290 mimic, the inhibitory effect of circCDR1 overexpression on proliferation was reversed by miR-1290 mimic (Figure 5(a,f)). As illustrated in Figure 5(b–c) and G-H, circCDR1 overexpression impeded cell migration and invasion, but miR-1290 mimic produced promotive effects and also reversed circCDR1 overexpression-induced inhibition. In addition, the apoptosis of KYSE-30 and TE-9 cells was induced by circCDR1 overexpression and reduced by miR-1290 mimic which also counteracted the facilitating effect of circCDR1 overexpression (Figure 5(d,i)). Furthermore, circCDR1 overexpression yielded down-regulation of miR-1290, whilst miR-1290 mimic up-regulated miR-1290 expression and reversed the effect of circDR1 overexpression (Figure 5e).

MiR-1290 reversed the effects of circCDR1 on the expressions of apoptosis/metastasis-related factors and anti-oncogenes in KYSE-30 and TE-9 cells

As the results described in Figure 6(a,c), and E, circCDR1 overexpression reduced and miR-1290 mimic enhanced the transcription and translation of Bcl-2 in the two cells, but those effects were inverse toward the transcription and translation of Bax and protein expression of C caspased-3. However, the impacts of circCDR1 overexpression on those apoptosis-related factors were reversed by miR-1290 mimic. Concerning the metastasis-
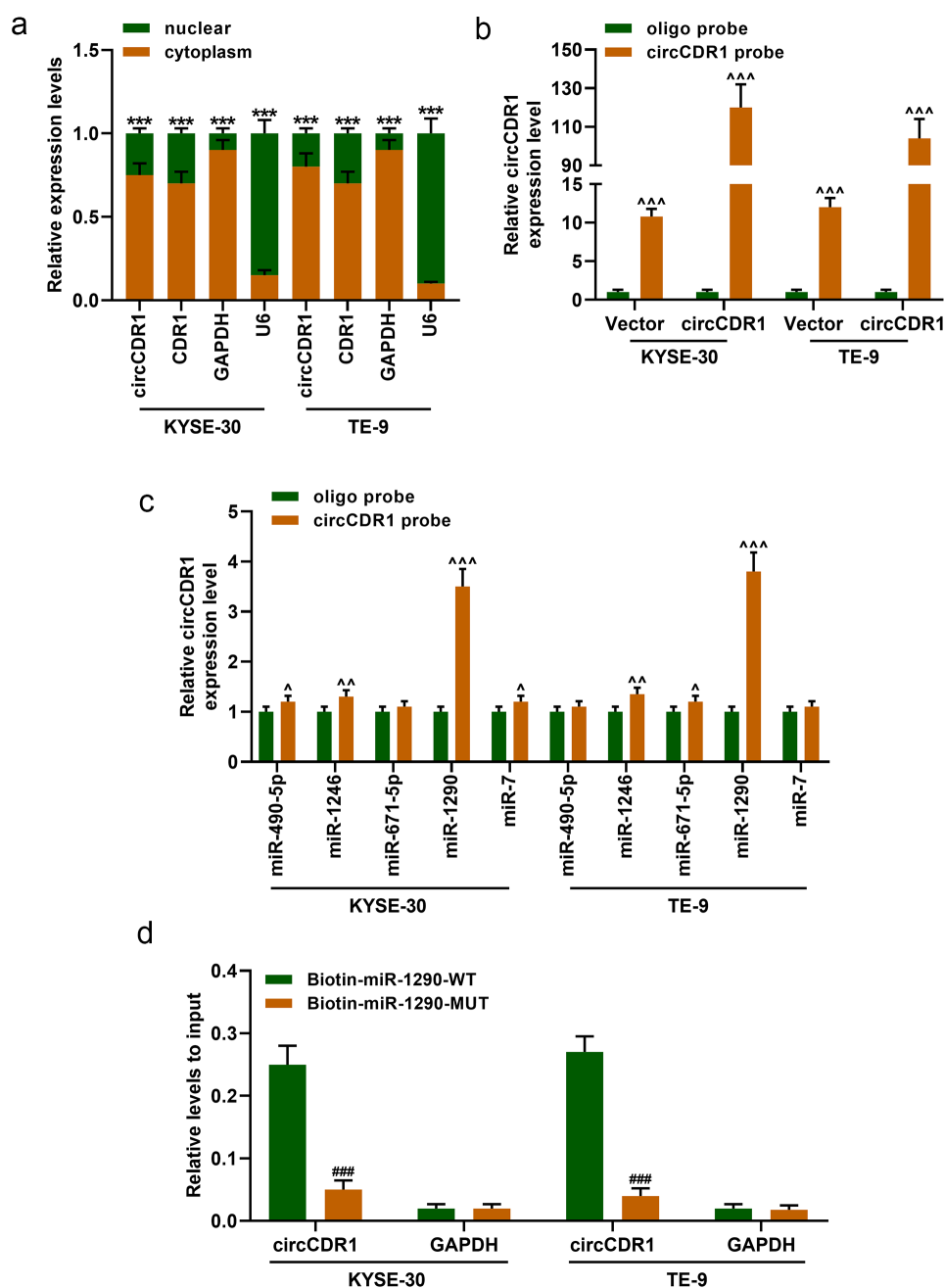
Figure 3. CircCDR1 mainly located in cytoplasm and could capture miR-1290 in KYSE-30 and TE-9 cells. (a) Relative circCDR1 and CDR1 expression levels in the cell cytoplasm or nucleus were examined by RT-qPCR. GAPDH was used as the cytoplasmic internal control, and U6 was used as the nuclear internal control. (b) Lysates from KYSE-30 and TE-9 cells with circCDR1 overexpression were subjected to biotinylated-circCDR1 pull-down assay and the expression level of circCDR1 was measured by RT-qPCR. GAPDH was used as an internal control. (c) The expressions of miRNAs were quantified by RT-qPCR after the biotinylated-circCDR1 pull-down assay in KYSE-30 and TE-9 cells. GAPDH was used as an internal control. (d) The miR-1290 expression level was quantified by RT-qPCR after the biotinylated-circCDR1 pull-down assay in KYSE-30 and TE-9 cells. GAPDH was used as an internal control. (***$P < 0.001$, vs. cytoplasm; ^$P < 0.05$, ^^$P < 0.01$, ^^^$P < 0.001$, vs. oligo probe; ###$P < 0.001$, vs. Biotin-miR-1290-WT). All experiments were conducted three times. (WT: wide type, MUT: mutation).

related factors (Figure 6(b,d,f)), circCDR1 overexpression down-regulated the transcription and translation levels of N-Cad and Vimentin and

promoted those of E-cad in the two cells, yet miR-1290 mimic oppositely impacted those factors, which also reversed the effects of circCDR1
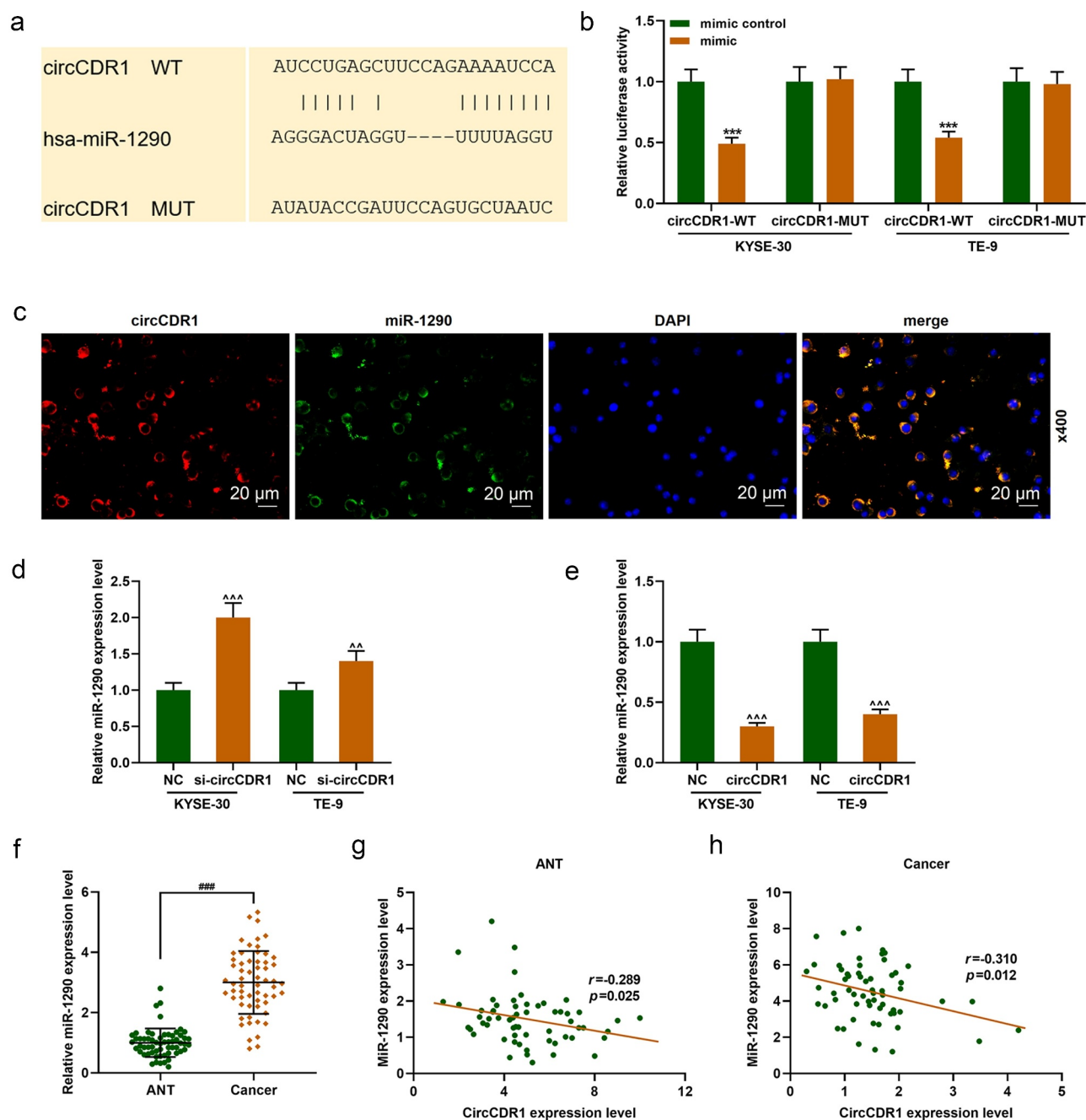
a

b

c

d

e

f

g

h

Figure 4. CircCDR1 had a negative correlation with high-expressed miR-1290 in ESCC tissues. (a) The putative binding site between miR-1290 and circCDR1 was predicted by CircInteractome. (b) Dual-luciferase reporter assay validated that circCDR1 sponged miR-1290 in KYSE-30 and TE-9 cells (***$P < 0.001$, vs. mimic control). (c) The binding relationship of circCDR1 and miR-1290 in A549 cells was detected by FISH. (d-e) The expression of miR-1290 in KYSE-30 and TE-9 cells was detected by RT-qPCR. U6 was used as an internal control (^^$P < 0.01$, ^^^$P < 0.001$, vs. NC). (f) The expression of miR-1290 in ANT and cancer tissues was detected by RT-qPCR. U6 was used as an internal control (###$P < 0.001$, vs. ANT). (g-h) The correlation of miR-1290 and circCDR1 in ANT and cancer tissues was analyzed by Pearson's correlation coefficient. All experiments were conducted three times. (ESCC: squamous cell cancer, FISH: fluorescence in situ hybridization, NC: negative control, ANT: adjacent normal tissues).

overexpression. Then, expressions of some key anti-oncogenes in the two cells were detected to explore whether the effects of circCDR1 and miR-1290 were mediated by regulating some or certain anti-oncogenes. In line with Figure 6(g), among the six anti-oncogenes, the transcription levels of IGFBP3, LHX6 and NFIX were facilitated by circCDR1 overexpression but dwindled by miR-
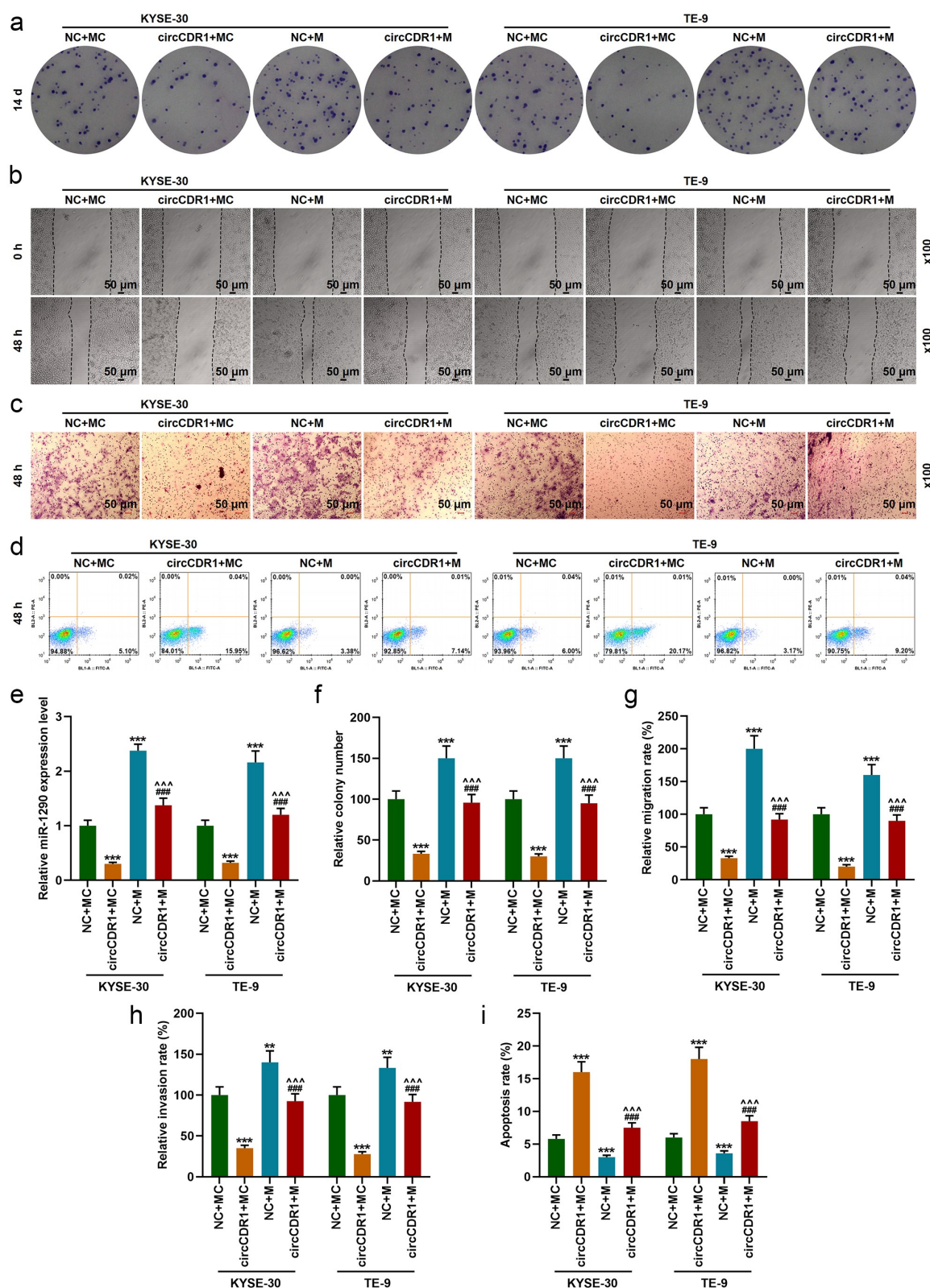
Figure 5. MiR-1290 reversed the effects of circCDR1 on the proliferation, apoptosis, migration, invasion, and miR-1290 expression of KYSE-30 and TE-9 cells. (a, f) The proliferation of KYSE-30 and TE-9 cells after transfection was detected by colony formation assay. (b, g) The migration of KYSE-30 and TE-9 cells after transfection was detected by wound-healing assay. (c, h) The invasion of KYSE-30 and TE-9 cells after transfection was detected by transwell assay. (d, i) The apoptosis of KYSE-30 and TE-9 cells after transfection was detected by flow cytometry. (e) The expression of miR-1290 in KYSE-30 and TE-9 cells after transfection was detected by RT-qPCR. U6 was used as an internal control. All experiments were conducted three times (**$P < 0.01$, ***$P < 0.001$, vs. NC+MC; ###$P < 0.001$, vs. NC+M; ^^^$P < 0.001$, vs. circCDR1+ MC). (NC: Negative control, MC: mimic control; M: mimic).
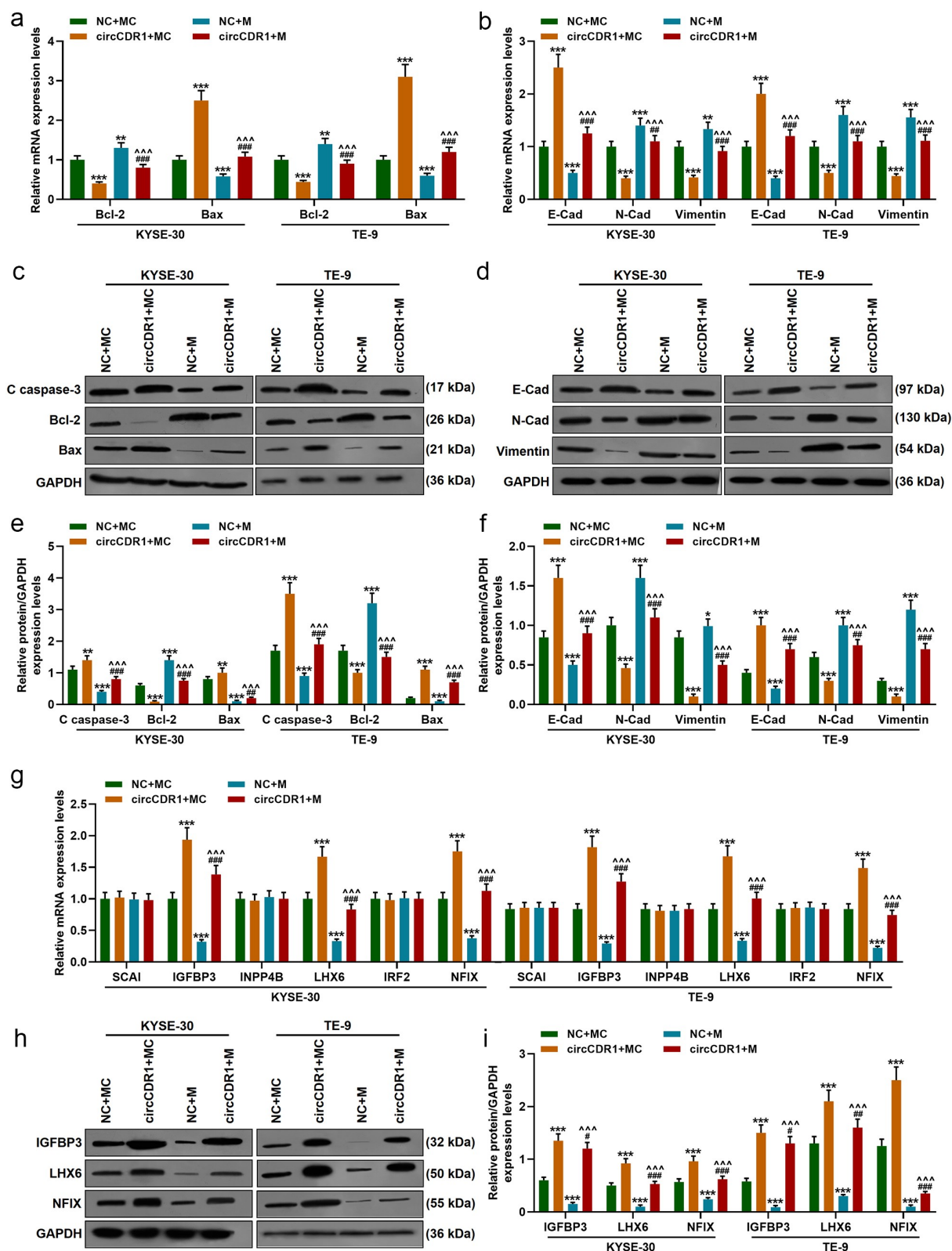
Figure 6. MiR-1290 reversed the effects of circCDR1 on the expressions of apoptosis/metastasis-related factors and anti-oncogenes in KYSE-30 and TE-9 cells. (a-b) The transcription levels of Bcl-2, Bax, E-Cad, N-Cad, and Vimentin in KYSE-30 and TE-9 cells after transfection were detected by RT-qPCR. GAPDH was used as an internal control. (c-f) The translation levels of Bcl-2, Bax, C caspase-3, E-Cad, N-Cad, and Vimentin in KYSE-30 and TE-9 cells after transfection were detected by western blot. GAPDH was used as an internal control. (g) The transcription levels of SCAI, IGFBP3, INPP4B, LHX6, IRF2, and NFIX in KYSE-30 and TE-9 cells after transfection were detected by RT-qPCR. GAPDH was used as an internal control. (h-i) The translation levels of IGFBP3, LHX6, and NFIX in KYSE-30 and TE-9 cells after transfection were detected by western blot. GAPDH was used as an internal control. All experiments were conducted three times ($^*P < 0.05$, $^{**}P < 0.01$, $^{***}P < 0.001$, vs. NC+MC; $^{###}P < 0.001$, vs. NC+M; $^{\wedge\wedge\wedge}P < 0.001$, vs. circCDR1+ MC). (NC: Negative control, MC: mimic control; M: mimic).

1290 mimic which could offset the results induced by circCDR1 overexpression. The exact binding relationship between miR-1290 and its down-regulated targets (IGFBP3, LHX6 and NFIX) was also mirrored in Supplementary Figure 2A-F. Therefore, we further gauged the translation levels of IGFBP3, LHX6 and NFIX in both KYSE-30 and TE-9 cells (Figure 6(h–i)), and the results were consistent with the transcription levels exhibited in Figure 6(g).

MiR-1290 reversed the effects of circCDR1 on tumor weight and volume, and on the expressions of apoptosis-related factors in the tumor tissues

A subcutaneous xenograft tumor model was constructed to verify the effects of circCDR1 and miR-1290 *in vivo* (Figure 7(a)). As clarified in Figure 7(b), the relative tumor weights were reduced by circCDR1 overexpression and enlarged by miR-1290 mimic, while such inhibitory effect of circCDR1 overexpression was reversed by miR-1290 mimic. According to Figure 7(c), the tumor volume was magnified, and the tumor growth was the fastest in NC+M group and the lowest in circCDR1+ MC group. In addition, the final volume of the tumors was the largest in NC+M group and the smallest in circCDR1+ MC group. Nevertheless, in circCDR1 + M group, the inhibitory effect of circCDR1 overexpression on the tumor volume was reversed by miR-1290 mimic. Furthermore, from Figure 7(d–f), it could be observed that circCDR1 overexpression decreased the gene and protein expressions of Bcl-2 and increased those of Bax and the protein expression of C caspase-3, but the impacts of miR-1290 mimic were opposite to and were able to countervail those of circCDR1 overexpression.

MiR-1290 reversed the effects of circCDR1 on the expressions of miR-1290 and Ki-67 in tumor tissues

The circCDR1 expression in the tumor tissues (Figure 8(a)) was detected to be remarkably up-regulated in circCDR1+ MC and circCDR1 + M groups but barely changed in NC+M group. The miR-1290 expression (Figure 8(b)) was down-regulated by circCDR1 overexpression and up-regulated by miR-1290 mimic, but such suppressive effect of circCDR1 overexpression was reversed by miR-1290 mimic. Finally, the expressions of the proliferation markers in the tissues were detected, as shown in Figure 8 (c,d) that Ki-67 expression was suppressed by circCDR1 overexpression and enhanced by miR-1290 mimic, whereas the inhibitory effect of circCDR1 was reversed by miR-1290 mimic.

Discussion

Evidence confirmed that aberrantly expressed circRNA is closely correlated to the development of many diseases and cancers including ESCC [9,15]. In addition, circCDR1 has been predicted to be low-expressed in ESCC [9]. Here, we further verified the prediction for the first time that circCDR1 was low-expressed both in ESCC tissues and cells. Considering that the structure of circRNA is a closed ring with a highly conservative sequence and is not easily digested by RNase [10], we detected the digestion level of circRNA after incubating RNAs with RNase, with the results revealing that RNase did not digest circCDR1. In line with the reports pointing out that circRNAs were highly stable [10,14,20], we not only found that circCDR1 was highly stable to the actinomycin D (transcription inhibitor) but also identified that circCDR1 was mainly located in the cytoplasm of the ESCC cells. Those findings demonstrated that the circCDR1 extracted from the ESCC cells had the basic characteristics as other circRNAs. Moreover, abnormal expression of circCDR1 in ESCC signified that circCDR1 might play a critical role in the development of ESCC, which also required further investigation.

Rapid proliferation and metastasis of cancer cells to normal tissues and insufficient apoptosis imposed great difficulties in cancer treatment [16,17]. The regulatory effect of circCDR1 on other cancers was also related to cell proliferation, invasion, and apoptosis [18,21]. Therefore, we focused on exploring the effects of circCDR1
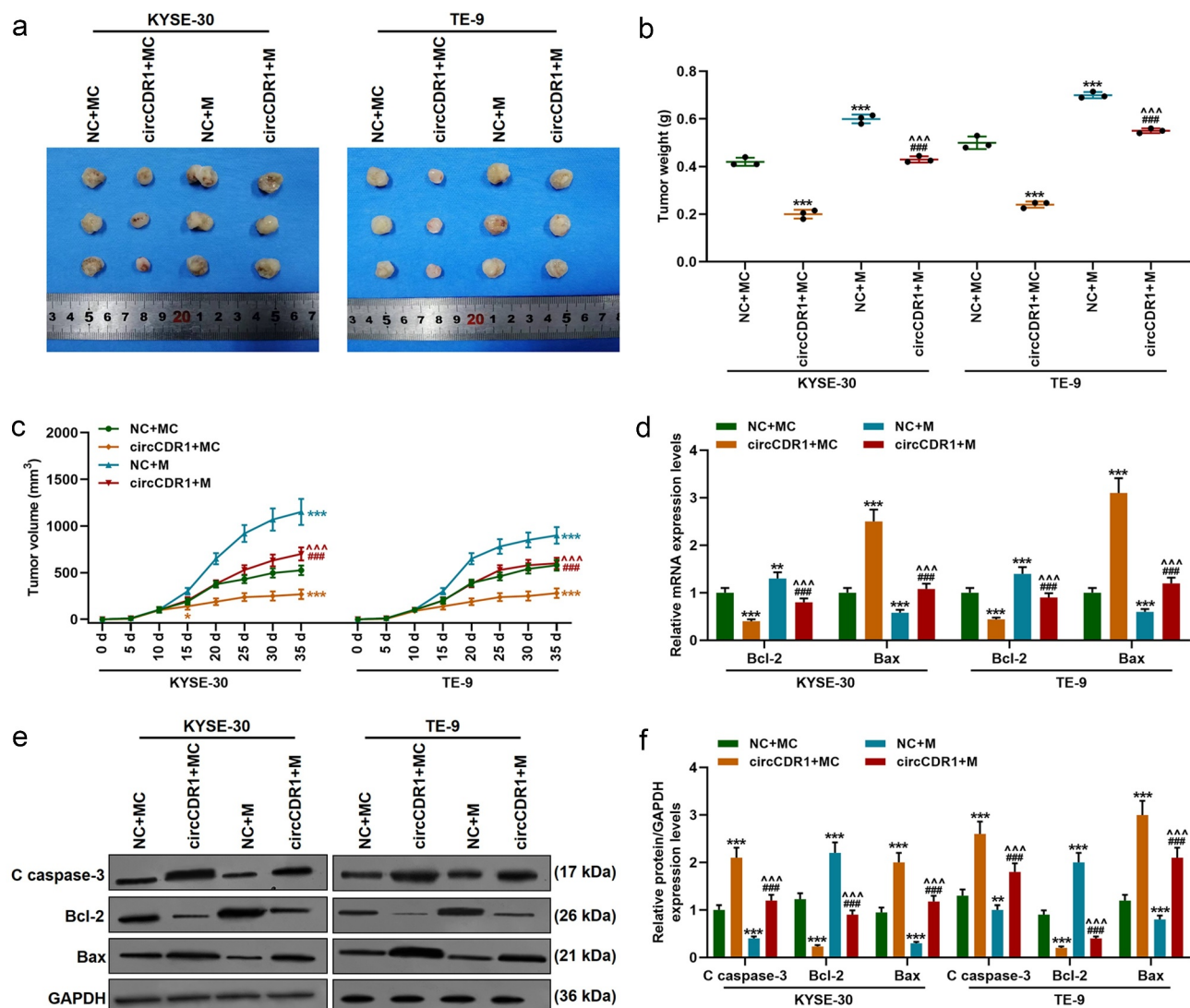
Figure 7. MiR-1290 reversed the effects of circCDR1 on tumor weight and volume, and on the expressions of apoptosis-related factors in tumor tissues. (a) The picture of solid tumor was exhibited. (b) The weight of solid tumor was calculated. (c) The volume of solid tumor was calculated. (d) The expressions of Bcl-2 and Bax in tumor tissues were detected by RT-qPCR. GAPDH was used as an internal control. (e-f) The expressions of C caspase-3, Bcl-2, and Bax in tumor tissues were detected by western blot. GAPDH was used as an internal control. All experiments were conducted three times (**$P < 0.01$, ***$P < 0.001$, vs. NC+MC; ###$P < 0.001$, vs. NC +M; ^^^$P < 0.001$, vs. circCDR1+ MC). (NC: Negative control, MC: mimic control; M: mimic). N = 8 per group.

on the proliferation and metastasis of ESCC cells, and discovered that circCDR1 inhibited the proliferation, migration, invasion, and apoptosis of ESCC cells. In recent years, the role of "miRNA sponge" has been a hot spot in the field of research [22]. p53-induced long non-coding RNA PGM5-AS1 inhibits the progression of esophageal squamous cell carcinoma through regulating miR-466/PTEN axis [3,23]. LINC00473 knockdown restrains the progression of esophageal squamous cell carcinoma through miR-497-5p/PRKAA1 axis [24]. In order to examine

whether there are miRNAs regulated by circCDR1, we screened five miRNAs, which have been reported to have regulatory effects on the biological functions of cancer cells [25,26] and uncovered that miR-1290 could bind with circCDR1. MiR-1290 was found to be abnormally expressed in many diseases, which therefore could act as a biomarker for cancers such as colorectal cancer, oral cancer, and pancreatic cancer [26–28]. As in ESCC, miR-1290 up-regulation is correlated with poor survival of patients [29]. Consistent with
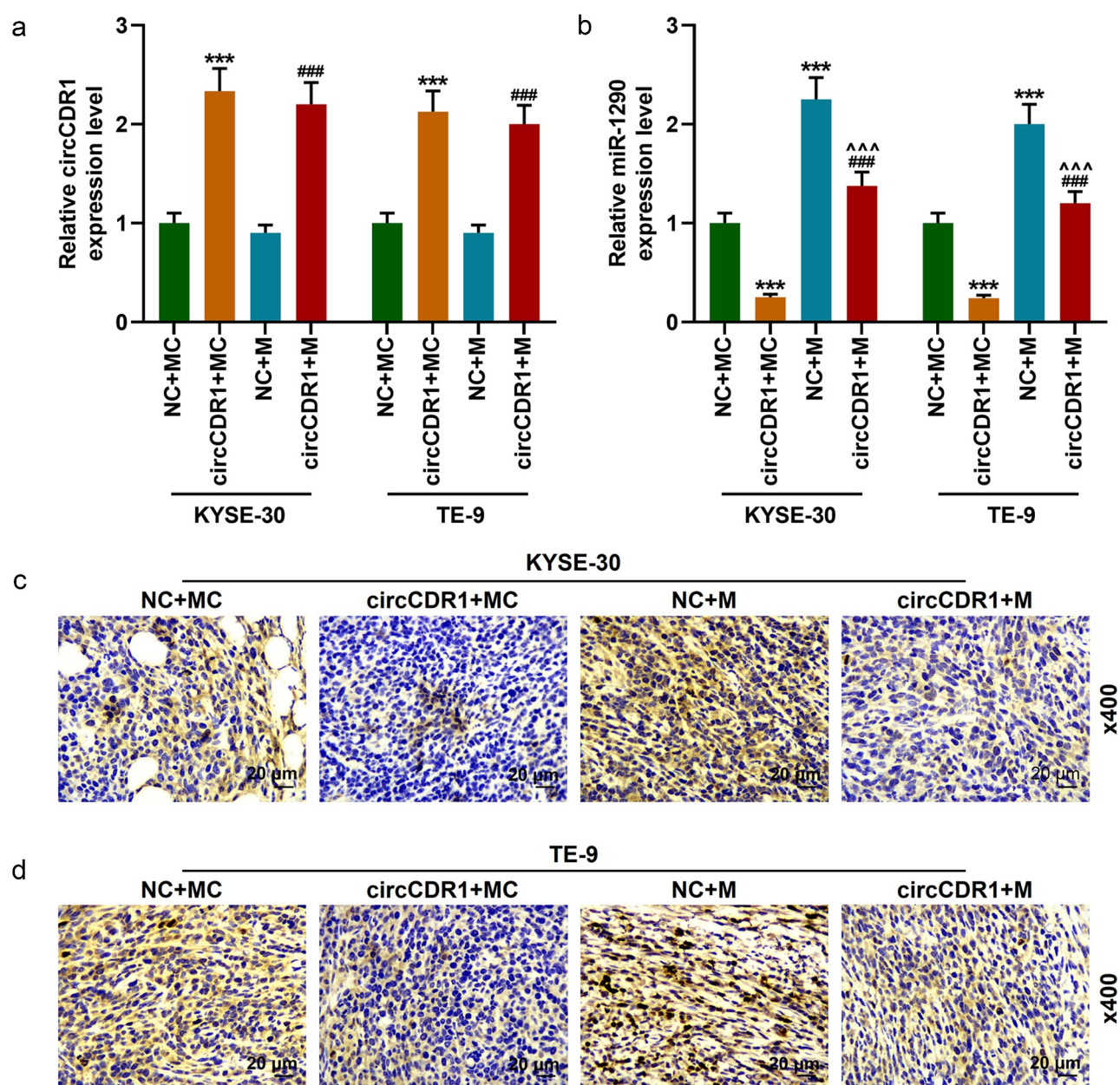
Figure 8. MiR-1290 reversed the effects of circCDR1 on the expressions of miR-1290 and Ki-67 in tumor tissues. (a) The expression of circCDR1 in tumor tissues was detected by RT-qPCR. GAPDH was used as an internal control. (b) The expression of miR-1290 in tumor tissues was detected by RT-qPCR. U6 was used as an internal control. (c-d) The expression of Ki67 in tumor tissues was detected by IHC. All experiments were conducted three times (**$P < 0.01$, ***$P < 0.001$, vs. NC+MC; ###$P < 0.001$, vs. NC+M; ^^^$P < 0.001$, vs. circCDR1+ MC). (NC: Negative control, MC: mimic control; M: mimic, IHC: immunohistochemical). N = 8 per group.

previous researches, we disclosed that miR-1290 was high-expressed in ESCC. In addition, the expression of miR-1290 was negatively correlated with circCDR1 level both in ESCC tissues and normal tissues, further indicating that the effect of circCDR1 on ESCC cells was associated with miR-1290. Thus, the effect of miR-1290 on ESCC cells was further detected, with the results unveiling that miR-1290 could promote the proliferation, migration, invasion, and apoptosis of ESCC cells and reverse the effect of circCDR1 on ESCC cells, but could not impact the expression of circCDR1. All these results corroborated that circCDR1 acted as a sponge of miR-1290 to regulate the biological functions of ESCC cells.

Researches put forward that miRNAs could target certain mRNAs to modulate disease development [30,31]. To probe into the

downstream mechanism deeper, the role of miR-1290 on the expressions of some anti-oncogenes in ESCC cells was examined. We unraveled that the transcription and translation levels of IGFBP3, LHX6, and NFLX could be regulated by miR-1290. The three low-expressed anti-oncogenes, IGFBP3, LHX6 and NFLX, could further regulate the activation of many signaling pathways and then modulate the cell biological functions [32–34]. Our results indicated that the effect of miR-1290 on ESCC cells might be mediated through regulating IGFBP3, LHX6, and NFLX. To confirm the present results, we established the subcutaneous xenotransplant tumor model in nude mice, which was usually used to prove the role of a certain gene on the growth of tumors [35]. The data verified that circCDR1 inhibited the growth and induced the apoptosis of the tumor, while miR-1290 had an opposite effect to circCDR1 and could reverse the effect of circDR1, which supported the *in vitro* results.

To conclude, our study authenticated that circCDR1 regulated the proliferation, migration, invasion, and apoptosis of ESCC cells by sponging miR-1290 *in vitro* and *in vivo*. Hence, circCDR1 may be used as a promising target and provide a new therapeutic method for ESCC.

Disclosure statement

No potential conflict of interest was reported by the author(s).

Funding

The author(s) reported that there is no funding associated with the work featured in this article.

Authors' contributions

Substantial contributions to conception and design: Yong Fang

Data acquisition, data analysis and interpretation: Jun Yin, Yaxing Shen, Hao Wang, Han Tang, Xiaosang Chen

Drafting the article or critically revising it for important intellectual content: Yong Fang

Final approval of the version to be published: Yong Fang, Jun Yin, Yaxing Shen, Hao Wang, Han Tang, Xiaosang Chen

Agreement to be accountable for all aspects of the work in ensuring that questions related to the accuracy or integrity of the work are appropriately investigated and resolved: Yong Fang, Jun Yin, Yaxing Shen, Hao Wang, Han Tang, Xiaosang Chen

References

[1] Palumbo A Jr., Meireles Da Costa N, Pontes B, et al. Esophageal cancer development: crucial clues arising from the extracellular matrix. Cells. 2020;9. DOI:10.3390/cells9020455.

[2] Ishikawa T, Yasuda T, Okayama T, et al. Efficacy and safety of early administration of pegfilgrastim in patients with esophageal cancer treated by docetaxel, cisplatin, and 5-fluorouracil (DCF): a phase 2 prospective study. Ann Oncol. 2019;30:4.

[3] Smyth EC, Lagergren J, Fitzgerald RC, et al. Oesophageal cancer. Nat Rev Dis Primers. 2017;3:17048.

[4] He Z, Ke Y. Precision screening for esophageal squamous cell carcinoma in China. Chin J Cancer Res. 2020;32:673–682.

[5] Oshikiri T, Takiguchi G, Hasegawa H, et al. Postoperative recurrent laryngeal nerve palsy is associated with pneumonia in minimally invasive esophagectomy for esophageal cancer. Surg Endosc. 2020;21:020–07455.

[6] Zhang K, Wu X, Wang J, et al. Circulating miRNA profile in esophageal adenocarcinoma. Am J Cancer Res. 2016;6:2713–2721.

[7] Zhou N, Hofstetter WL. Prognostic and therapeutic molecular markers in the clinical management of esophageal cancer. Expert Rev Mol Diagn. 2020;18:1731307.

[8] Zhang J, Li D, Wang D, et al. CircRNA expression profiles in human dental pulp stromal cells undergoing oxidative stress. J Transl Med. 2019;17:327.

[9] Fan L, Cao Q, Liu J, et al. Circular RNA profiling and its potential for esophageal squamous cell cancer diagnosis and prognosis. Mol Cancer. 2019 Jan 23;18(1):16.

[10] Xia Q, Ding T, Zhang G, et al. Circular RNA expression profiling identifies prostate cancer- specific circRNAs in prostate cancer. Cell Physiol Biochem. 2018;50:1903–1915.

[11] Xu D, Wu Y, Wang X, et al. Identification of functional circRNA/miRNA/mRNA regulatory network for exploring prospective therapy strategy of colorectal cancer. J Cell Biochem. 2020;1:29703.

[12] Yang SJ, Wang DD, Zhou SY, et al. Identification of circRNA-miRNA networks for exploring an underlying prognosis strategy for breast cancer. Epigenomics. 2020;12:101–125.

[13] Liu J, Li Z, Teng W, et al. Identification of down-regulated circRNAs from tissue and plasma of patients with gastric cancer and construction of a circRNA-miRNA-mRNA network. J Cell Biochem. 2020;13:29673.

[14] Wu P, Mo Y, Peng M, et al. Emerging role of tumor-related functional peptides encoded by lncRNA and circRNA. Mol Cancer. 2020;19:020–1147.

[15] Huang E, Fu J, Yu Q, et al. CircRNA hsa_circ_0004771 promotes esophageal squamous cell cancer progression via miR-339-5p/CDC25A axis. Epigenomics. 2020;13:2019–2404.

[16] Xiang Z, Xu C, Wu G, et al. CircRNA-UCK2 increased TET1 inhibits proliferation and invasion of prostate cancer cells via sponge MiRNA-767-5p. Open Med. 2019;14:833–842.

[17] Li X, Lin S, Mo Z, et al. CircRNA_100395 inhibits cell proliferation and metastasis in ovarian cancer via regulating miR-1228/p53/epithelial-mesenchymal transition (EMT) axis. J Cancer. 2020;11:599–609.

[18] Yao Y, Hua Q, Zhou Y, et al. CircRNA has_-circ_0001946 promotes cell growth in lung adenocarcinoma by regulating miR-135a-5p/SIRT1 axis and activating Wnt/beta-catenin signaling pathway. Biomed Pharmacothe. 2019;111:1367–1375.

[19] Li X, Diao H. Circular RNA circ_0001946 acts as a competing endogenous RNA to inhibit glioblastoma progression by modulating miR-671-5p and CDR1. J Cell Physiol. 2019;234:13807–13819.

[20] Zhu Z, Ma Y, Li Y, et al. The comprehensive detection of miRNA, lncRNA, and circRNA in regulation of mouse melanocyte and skin development. Biol Res. 2020;53:020–0272.

[21] Li Y, Zhang J, Pan S, et al. CircRNA CDR1as knockdown inhibits progression of non-small-cell lung cancer by regulating miR-219a-5p/SOX5 axis. Thorac Cancer. 2020;11:537–548.

[22] Huang C, Deng H, Wang Y, et al. Circular RNA circABCC4 as the ceRNA of miR-1182 facilitates prostate cancer progression by promoting FOXP4 expression. J Cell Mol Med. 2019;23:6112–6119.

[23] Pennathur A, Gibson MK, Jobe BA, et al. Oesophageal carcinoma. Lancet (London. England). 2013;381:400–412.

[24] He Z. LINC00473/miR-497-5p regulates esophageal squamous cell carcinoma progression through targeting PRKAA1. Cancer Biother Radiopharm. 2019;34:650–659.

[25] Liu H, Zhang Q, Lou Q, et al. Differential analysis of lncRNA, miRNA and mRNA expression profiles and the prognostic value of lncRNA in esophageal cancer. Pathol Oncol Res. 2019;10:019–00655.

[26] Liu X, Xu X, Pan B, et al. Circulating miR-1290 and miR-320d as novel diagnostic biomarkers of human colorectal cancer. J Cancer. 2019;10:43–50.

[27] Qin WJ, Wang WP, Wang XB, et al. MiR-1290 targets CCNG2 to promote the metastasis of oral squamous cell carcinoma. Eur Rev Med Pharmacol Sci. 2019;23:10332–10342.

[28] Tavano F, Gioffreda D, Valvano MR, et al. Droplet digital PCR quantification of miR-1290 as a circulating biomarker for pancreatic cancer. Sci Rep. 2018;8(1):16389.

[29] Sun H, Wang L, Zhao Q, et al. Diagnostic and prognostic value of serum miRNA-1290 in human esophageal squamous cell carcinoma. Cancer Biomark. 2019;25:381–387.

[30] Sun Y, Ju XL, Li D, et al. Luo RH. miR-1290 promotes proliferation and suppresses apoptosis in acute myeloid leukemia by targeting FOXG1/SOCS3. J Biol Regul Homeost Agents. 2019;33:1703–1713.

[31] Chen JY, Xu LF, Hu HL, et al. MiRNA-215-5p alleviates the metastasis of prostate cancer by targeting PGK1. Eur Rev Med Pharmacol Sci. 2020;24:639–646.

[32] Chen G, Zhou X, Xu Z. Effects of IGFBP3 gene silencing mediated inhibition of ERK/MAPK signaling pathway on proliferation, apoptosis, autophagy, and cell senescence in rats nucleus pulposus cells. J Cell Physiol. 2019;234:9308–9315.

[33] Bi QJ, Men XJ, Han R, et al. LHX6 inhibits the proliferation, invasion and migration of breast cancer cells by modulating the PI3K/Akt/mTOR signaling pathway. Eur Rev Med Pharmacol Sci. 2018;22:3067–3073.

[34] Hall T, Walker M, Ganuza M, et al. Nfix promotes survival of immature hematopoietic cells via regulation of c-Mpl. Stem Cells. 2018;36:943–950.

[35] Zeng K, Chen X, Xu M, et al. CircHIPK3 promotes colorectal cancer growth and metastasis by sponging miR-7. Cell Death Dis. 2018;9. DOI:10.1038/s41419-018-0454-8.